buildings

MDPI

Article

Insights on the Mortars of Ancient Roman Aqueducts: *Aqua Virgo* and Aqueduct Y, Rome (Italy)

Laura Calzolari [1,*], Maria Elisa Amadasi [2], Laura Medeghini [1] and Silvano Mignardi [1]

[1] Department of Earth Sciences, Sapienza University of Rome, Piazzale A. Moro, 5, 00185 Rome, Italy; laura.medeghini@uniroma1.it (L.M.); silvano.mignardi@uniroma1.it (S.M.)
[2] Department of Science of Antiquities, Sapienza University of Rome, Piazzale A. Moro, 5, 00185 Rome, Italy; amadasi.mariaelisa@gmail.com
* Correspondence: laura.calzolari@uniroma1.it

Abstract: Despite the archaeological importance of *Aqua Virgo*, a Roman aqueduct built in 19 BC and still functioning nowadays, there is a lack of information about the mortars coming from the inner duct. This work aims to investigate the mortars from *Aqua Virgo* and Aqueduct Y, an unidentified aqueduct running under the first one in the La Rinascente area (between Via del Nazareno and Via dei Due Macelli, Rome, IT) through Optical Microscopy (OM), X-ray Powder Diffraction (XRPD) and Scanning Electron Microscopy with Energy Dispersive Spectroscopy (SEM-EDS). The aim is to understand which materials guarantee such longevity and differentiate between different intervention phases. Local natural materials with pozzolanic behaviour—in particular, Pozzolane Rosse—and ceramic fragments are widely employed, mixed or not, for the realisation of the hydraulic mortars under investigation, independently of the intervention phase. Of particular interest is the discovery of an amorphous binder composed of Si, Al, Ca, K and Mg in some samples characterised by the absence of calcite.

Keywords: Roman aqueducts; archaeometry; mortars; geomaterials in cultural heritage

Citation: Calzolari, L.; Amadasi, M.E.; Medeghini, L.; Mignardi, S. Insights on the Mortars of Ancient Roman Aqueducts: *Aqua Virgo* and Aqueduct Y, Rome (Italy). *Buildings* **2024**, *14*, 69. https://doi.org/10.3390/buildings14010069

Academic Editor: Linda Giresini

Received: 24 October 2023
Revised: 12 December 2023
Accepted: 23 December 2023
Published: 26 December 2023

1. Introduction

Aqua Virgo is the oldest aqueduct still functioning in Rome. Although it was inaugurated in 19 BC, it still collects water from the ancient springs in Salone and its *terminus* is located in *Campus Martius*, in the vicinity of Pantheon (Figure 1) [1]. The source area is about 20 km east of the city centre in a marshy area described by Frontinus as *palustribus locis* and located at the eighth mile of the ancient Via Collatina [2].

Apart from the arcades in the city centre and a few substructions or short series of arches, *Aqua Virgo* runs underground [3]. This is possible due to the underlying bedrock being Pozzolane Rosse and tuff [4].

During the 6th century, especially following the Gothic Wars, *Aqua Virgo*, as well as the other Roman aqueducts, was damaged. However, while all the other aqueducts were heavily destroyed and left to decay, *Aqua Virgo* continued to supply the city [5]. In 1570, under the papacy of Pius V, *Aqua Virgo* was finally restored in its entirety: the main sources in Salone were identified and unclogged, and the entire channel was repaired and reactivated. Until then, only the last portion, downstream of Villa Ada, closer to the city and of easier access, was addressed for maintenance and restoration works [6,7]. By the end of the 19th century, *Aqua Virgo* was still flowing freely inside the original channel. But in 1887, the final part downstream of Villa Medici was interrupted, and the waterflow was diverted into a new and safer system, which would ensure the constant distribution of water [8].

On one side, the almost entirely underground route, as well as the constant presence of water, has made access to the aqueduct either challenging or impossible. On the other side, the continuous activity of the aqueduct has allowed the preservation of the structure and

permitted a regular flow throughout the centuries. For this reason, *Aqua Virgo* represents an ideal case study for the identification of the hydraulic techniques and the building materials employed in the Roman aqueducts and in the successive phases of intervention to guarantee the functioning. Recent investigations inside the channel enabled, for the first time, the sampling, and hence the analysis, of hydraulic mortar from the inner channel.

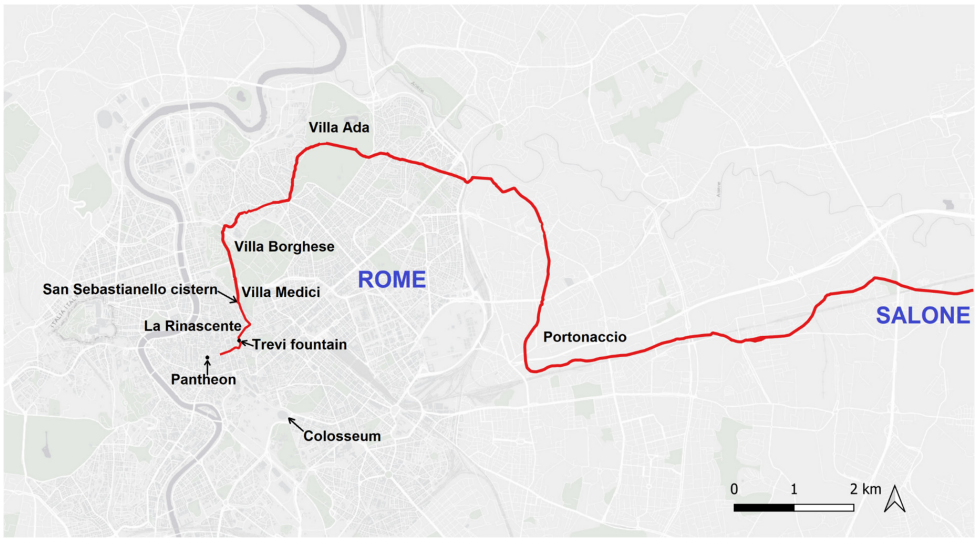

Figure 1. Map of the path of *Aqua Virgo*, from the springs in Salone until the *terminus* in *Campus Martius* (QGIS elaboration).

Due to the precarious safety conditions, it has now been feasible to take mortar samples only in two separate parts of the aqueduct: a section under Villa Medici and one in the La Rinascente area (Figure 2).

During the excavations at La Rinascente mall (2009–2016), another aqueduct below *Aqua Virgo* has been individuated for an extension of about 80 m. This aqueduct is not mentioned either in the ancient literature or in the antiquarian documents, so the interpretation of its features, route, and provenience of the water remains complex and uncertain. The aqueduct is traditionally called "Aqueduct Y" and probably dates to the early Augustan period before the construction of *Aqua Virgo*, which stands on top of it in the La Rinascente area. In this stretch, the *specus* of Aqueduct Y is about 140 cm wide and presents walls and a vault in masonry, alternatively built in *opus quadratum* of tuff blocks and *opus reticulatum*. The bottom is faced with *cocciopesto* [9,10]. There is a point in which the *specus* is accessible, as the duct has been cut, and so its section is visible.

In the city of Rome, eleven aqueducts were built in the Roman period to supply water for the increasing population and needs of the society, and the majority of them are still present as archaeological ruins [11]. However, there is a lack of archaeometric investigations about the mortars that made them so durable [12]. Even broadening the research to the aqueducts built all over the Roman empire, not many archaeometric investigations have been carried out on their mortars [13–18]. What we know thanks to historical sources [19] and scientific studies carried out on other types of structures is that Ancient Romans commonly used lime, which is an aerial binder combined with aggregates with pozzolanic behaviour that can be differentiated in artificial (such as ceramic fragments) and natural (such as pozzolan) [20]. Another possibility is to calcinate marly limestone [21], but it is less common. The main revolution in mortar production happened when, at the end of the 18th century, Joseph Parker patented the "Roman cement", which later led to the production of Portland cement [22].

Concerning masonry techniques, ancient Romans used several types of combinations of materials, applying different masonry patterns in order to adapt them to the specific needs of the architectonic structure [23]. Just to list some of the most common, they used

opus reticulatum, in which stones cut as pyramids with square bases were used as vestment of the wall in *opus caementicium*, which is the concrete used to build the core of the walls, composed of lime-pozzolan mortar mixed with big fragments of rock. Another very common type is *opus latericium*, in which the stone's pyramids of *opus reticulatum* are substituted by bricks [20,24]. For structures that were in contact with water, ancient Romans used a covering layer in *cocciopesto*, a type of mortar characterised by the presence of crushed ceramic [20,25]. Investigating the mortars employed in the inner ducts of aqueducts will give further information on the materials that guarantee hydraulicity to the masonry structures.

Figure 2. Map of the areas of sampling and photos of the inner duct of *Aqua Virgo*. Satellite images are taken from Google Earth and QGIS elaboration of *Aqua Virgo* path using ACEA Ato2 topographical survey, the reconstructive hypothesis of the route of *Aqua Virgo* presented by Montalbano [26] and new data obtained from speleological investigations inside the channel (Gruppo Speleo Archeologico Vespertilio).

Considering the span of the lifetime of *Aqua Virgo*, which made it an incredibly durable artefact, and the lack of information about Aqueduct Y, the aim of this research is to apply a multi-analytical approach to investigate the mortars from the inner duct of both aqueducts. The archaeometric characterisation aims to obtain a better understanding of the different intervention phases that occurred by comparing the different materials used to formulate the mortars.

2. Materials and Methods

2.1. Materials

The mortar samples analysed were collected in the inner ducts of *Aqua Virgo* and the so-called Aqueduct Y (Table 1). Two are the areas of sampling, both located in the city centre of Rome (Figure 2). The first area is located under Villa Medici: *Aqua Virgo*, which runs at a depth of about 22 m below the Pincian Hill, can be accessed from a spiral staircase built during the 16th century. The vaulted channel is about 150 cm wide and 230 cm high. In the stretch that runs from the staircase in the direction of the San Sebastianello cistern, ten samples have been collected (from VIR1 to VIR10). This portion of the *specus* is the final part of the aqueduct with a free surface flow. The second area of sampling is located between Via del Nazareno, Via del Tritone, and Via dei Due Macelli, under the building that nowadays holds the "La Rinascente" shopping mall (Figure 2). Originally, in this area, the aqueduct ran on the surface on top of arches. Now the arcades, mainly hidden by the urban expansion, can still be seen under La Rinascente mall, where they have recently been brought to light, and in a few other points towards the Trevi fountain [9]. Here, the samples have been collected from *Aqua Virgo* and Aqueduct Y in an area in which they are both dismissed. Samples from VIR11 to VIR17 have been taken from the inner *specus* of *Aqua Virgo*, in the stretch that runs from Via del Nazareno and proceeding onward Via dei Due Macelli. Samples from 1Y to 3Y have been collected from the inner duct of Aqueduct Y, which runs below *Aqua Virgo*.

2.2. Methods

The archaeometric characterisation of the samples followed a multi-analytical approach, giving information on the type of binder and the nature of the aggregate. Moreover, the detection of the crystalline phases present in the sample and the characterisation of the amorphous ones (related to the binder) were obtained.

Initially, the samples were observed using a Dino-Lite Digital Microscope and DinoCapture 2.0 software (see Table S1). For each sample, thin sections were realised to perform petrographic investigation with Optical Microscopy (OM). The observations were carried out with a Leica DM750 P microscope, a Leica MC190 HD video camera, and LAS V4 4.12 software. For the description of the mortar samples, guidelines from [27,28] were followed, describing the binder, aggregate, binder-to-aggregate ratio, porosity, the eventual presence of lumps and admixtures.

Each sample was also finely grinded in an agate mortar to be analysed with X-ray Powder Diffraction (XRPD) in order to detect the crystalline phases present in both binder and aggregate. The diffractometer used is a Bruker D8 focus diffractometer with CuKα radiation, operating at 40 kV and 30 mA. The instrumental set-up used has a 3–60° 2θ range and a scan step of 0.02° 2θ/2 s. Data processing, including semi-quantitative analysis based on the "Reference Intensity Ration Method", was performed using XPowderX Ver. 2019.01.01 software [29].

A selection of 8 representative samples from *Aqua Virgo* (VIR1, VIR6, VIR7, VIR10, VIR13, VIR14, VIR15, VIR16) was analysed using Scanning Electron Microscopy with Energy-Dispersive X-ray Spectroscopy (SEM-EDS) on thin sections to deeply investigate the microstructure of the aggregate and its composition, as well as the ones of the binder and their interactions. The analysis was performed on thin sections already analysed at OM and metallised with graphite, using a FEI Quanta 400 scanning electron microscope, and images were collected in Backscattered Electron Mode (BSE).

Table 1. List of samples.

Sample	Type	Description
		Villa Medici
VIR1	Bedding mortar between bricks.	Collected from the left lateral wall, a few meters from the spiral staircase.
VIR2	Covering layer—plaster.	Collected from the left lateral wall. It is the layer that covers the brick wall where sample VIR1 has been collected.
VIR3	Mortar between stone blocks.	Left wall, close to VIR1 and 2. This part of the wall is not smooth; there are protruding stone blocks. The area has been interpreted as a possible occlusion.
VIR4	Mortar from a well.	Mortar covering the circular well, probably Roman period.
VIR5	Mortar from the vault.	Collected close to the circular well of VIR4. Probably Roman period.
VIR6	Mortar from the vault.	Collected close to VIR5 from a layer that is beneath it. Probably Roman period.
VIR7	Covering layer—plaster.	From the right lateral wall. Incised date "1742".
VIR8	Covering layer—plaster.	From the right lateral wall. Incised date "1650".
VIR9	Mortar between stone blocks.	From the left lateral wall, inferior part. Below VIR10.
VIR10	Covering layer—plaster.	From the left lateral wall, upper part. Above VIR9.
		La Rinascente
VIR11	Bedding mortar between bricks.	From the left lateral wall, 80 cm up with respect to the base of the duct covered with calcareous sediments due to the water flow.
VIR12	Mortar from the inner part of the wall.	From the left lateral wall, collected from a hole a few cm deep, above VIR11, 1 m *circa* from the base of the duct.
VIR13	Covering layer—plaster.	From the left lateral wall, superficial, above VIR12.
VIR14	Covering layer—plaster.	From the right lateral wall, close to a water box. Incised date "1651".
VIR15	Mortar from the inner part of the wall.	From the right lateral wall, collected between bricks, in a breach in the wall. A lead pipe is also visible.
VIR16	Covering layer—plaster.	From the left lateral wall.
VIR17	Mortar from the vault.	In the junction point between lateral wall and vault.
1Y	*Cocciopesto*.	Covering layer from the left lateral wall. Ceramic fragments reaching centimetric size are visible to naked eye.
2Y	*Cocciopesto*.	Collected in the junction between the lateral wall (left) and the base of the duct. Ceramic fragments reaching centimetric size are visible to naked eye.
3Y	*Cocciopesto*.	Base of the duct. Ceramic fragments reaching centimetric size are visible to naked eye.

3. Results

3.1. Optical Microscopy

The main features obtained by petrographic characterisation are described in the text hereafter, whereas the detailed description of each sample is reported in Table S2.

3.1.1. Villa Medici

The samples coming from this area can be distinguished into six groups. Samples VIR1 and VIR2 belong to group 1, as they are characterised by the presence of pozzolan and an amorphous binder. Sample VIR3 is different from the previous ones because of the presence of rock fragments containing feldspar and clinopyroxene, and it constitutes a group by itself (group 2). Samples VIR4, VIR 5 and VIR 6 are part of group 3 and are characterised by a calcic lime binder and pozzolan. VIR7 constitutes a group by itself (group 4) as it is composed of three strata, and the inner one contains flint. VIR8 belongs to group 5 and is characterised by an amorphous binder and the presence of ceramic fragments. Group 6, which comprises samples VIR9 and VIR10, differs from group 1 because, in this group, only Pozzolane Rosse is present, whereas in group 1, Pozzolane Nere is also present.

Samples VIR1 and VIR2 have a homologous composition: amorphous binder (Figure 3a) with a light brown colour in XPL and an aggregate mainly constituted by natural materials with pozzolanic behaviour, in particular, of pozzolans from the Colli Albani Volcanic District. Among the pyroclastic rock fragments, it is possible to distinguish between Pozzolane Rosse and Pozzolane Nere. Indeed, the former has a low porphyritic index, presenting

a cryptocrystalline groundmass with leucite microcysts with star-like habit and irregular porosities (Figure 4a,b), whereas the latter differs from the first one because of the presence of leucite with euhedral–subhedral habit, compatible with Pozzolane Nere characteristics. The binder-to-aggregate ratio in both samples is 1:3. Sample VIR3 differs from VIR1 and VIR2 by the presence of holocrystalline rock fragments constituted by crystals of feldspar and clinopyroxene.

Sample VIR4, VIR5 and VIR6 present a calcic lime binder with micritic to microsparitic texture (Figure 3b), which is the main difference with samples from group 1, as the aggregate is mainly composed of natural materials with pozzolanic behaviour, specifically Pozzolane Rosse (Figure 4c) and Pozzolane Nere. Some of the pyroclastic rock fragments sometimes show a small portion of glass, yellow in colour. The binder-to-aggregate ratio is 1:3. Moreover, close to VIR6, a rounded white stone aggregate, 1 mm in diameter, was collected. Similar aggregates were visible also on the surface of samples VIR4 and VIR5. Analysis of thin sections revealed it is a sedimentary carbonate rock, with micrite groundmass and a few veins with sparitic calcite, classifiable as wackestone.

Sample VIR7 differs from all the previously described samples. It comes from the right lateral wall, at a point where the labourers incised the date "1742" on the still-fresh covering layer. It is characterised by three strata, numbered from the most external (1) to the inner one (3) (Figure 3c). The first layer, whose maximum thickness is 230 µm, is only composed of calcite, from micritic to sparitic. The second layer has a calcic lime binder, constituted by micritic calcite, not homogeneous, and the aggregate is mainly composed of Pozzolane Rosse, and single crystals of clinopyroxene are dispersed in the binder. At the interface between the second and third layers, calcite is present due to secondary reprecipitation. The third layer differs from the second because the calcic lime binder, with micritic calcite, looks more compact. Some Pozzolane Rosse scoriae are present (and they constitute the fine fraction of the aggregate), but the biggest aggregate is constituted by a flint fragment, recognisable thanks to the cryptocrystalline silica structure (Figure 4d).

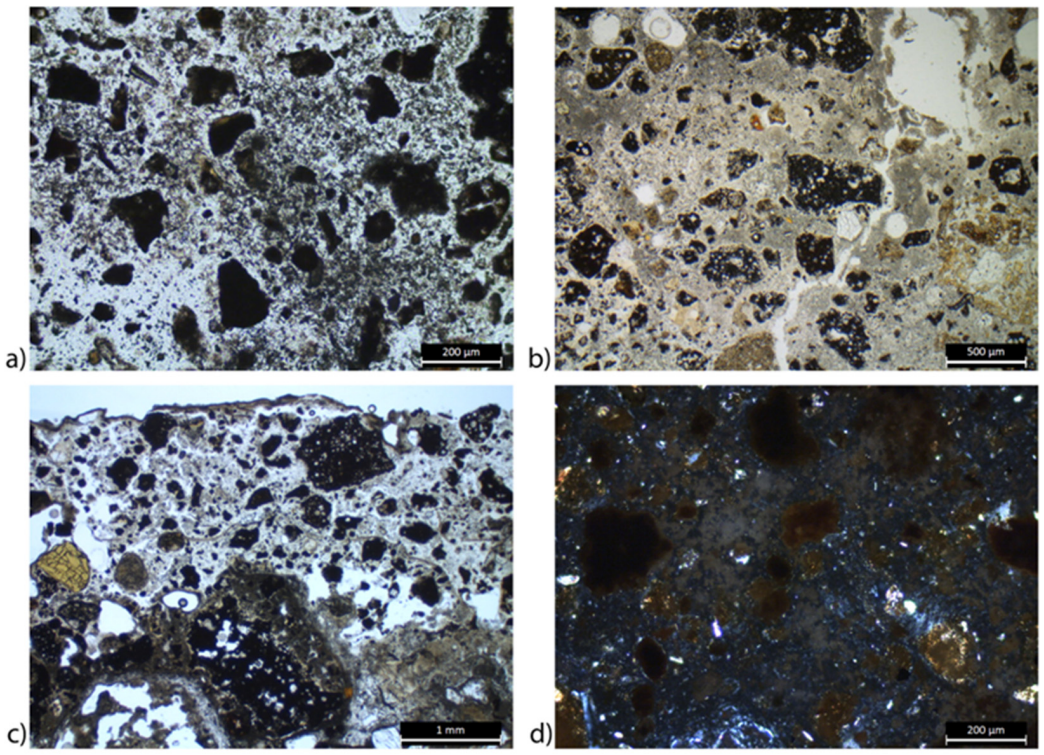

Figure 3. *Cont.*

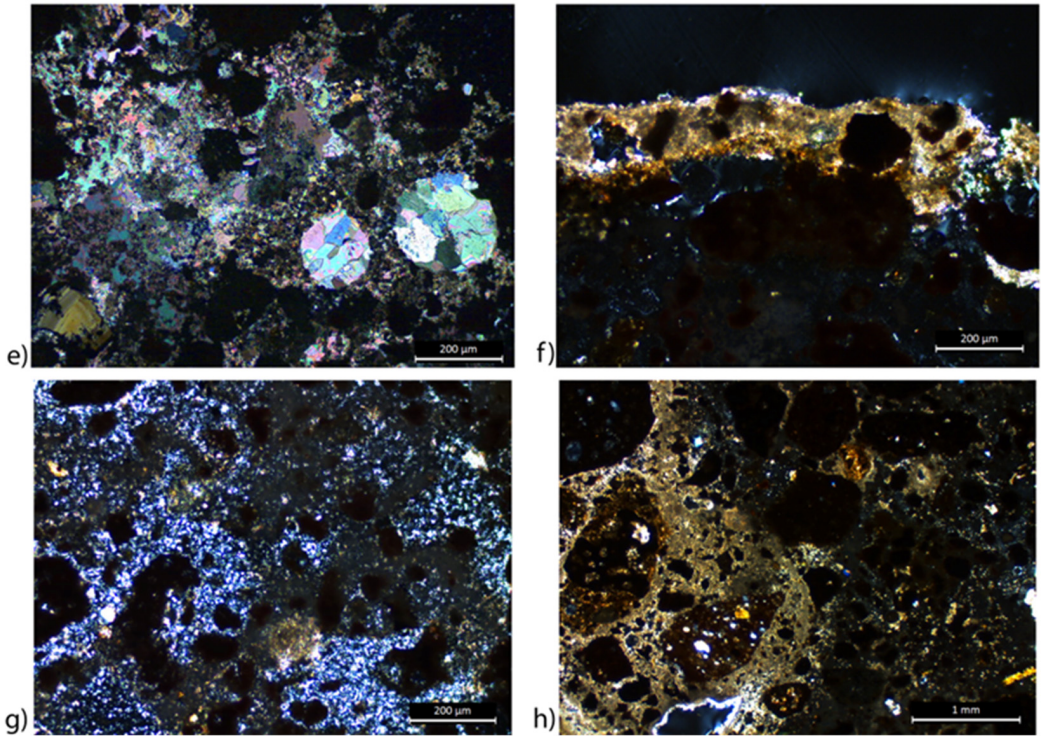

Figure 3. Images at OM of the binder fraction of samples from *Aqua Virgo*. (**a**) Amorphous binder, with the finest fraction of aggregate, in sample VIR2, at PPL. (**b**) Calcic lime binder in sample VIR5 at PPL. (**c**) Stratigraphic image at PPL of sample VIR7: on top, there is layer 1, very thin with respect to the other two, which can be distinguished by the compactness of the binder. Calcite due to secondary reprecipitation is visible at bottom right. (**d**) Amorphous binder at XPL, characterised by a brownish colour (sample VIR8). (**e**) Secondary calcite filling porosities in sample VIR12 and substituting part of the binder (XPL). (**f**) Sample VIR14, with a superficial layer (1st) characterised by calcic lime binder and a second layer with amorphous binder (XPL). (**g**) Microsparitic calcite constituting the binder of sample VIR15 (XPL). (**h**) Sample VIR16: on the left the calcic lime binder of the second layer; on the right, the amorphous binder of the first layer (XPL).

Sample VIR8 was collected close to an incision reporting the date 1650. The binder is amorphous (Figure 3d), and the major component of the aggregate is constituted by artificial materials with pozzolanic behaviour, i.e., ceramic fragments (Figure 3e). The finest fraction of the aggregate is a mix of natural and artificial materials with pozzolanic behaviour, with medium dimension around 100 µm. The binder-to-aggregate ratio is 1:2.

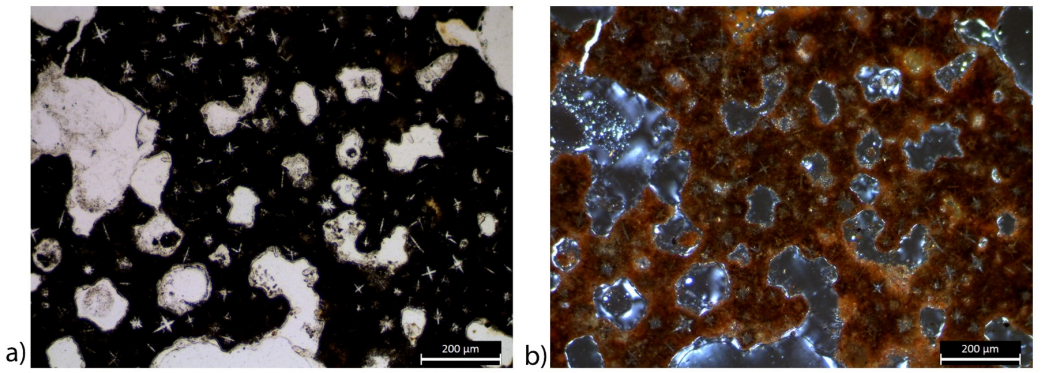

Figure 4. *Cont.*

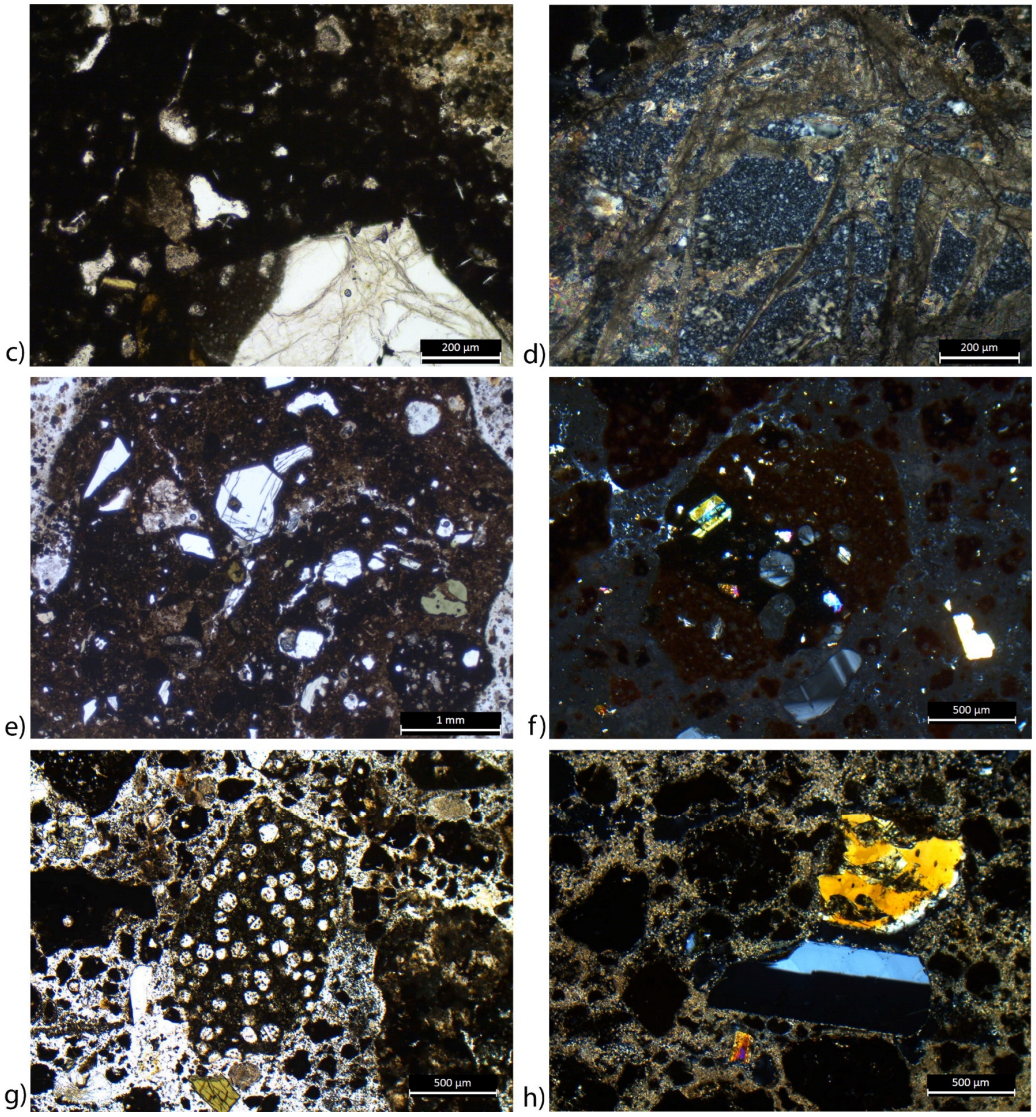

Figure 4. Images at OM of the aggregate fraction of samples from *Aqua Virgo*. (**a**,**b**) Sample VIR1 Pozzolane Rosse scoria, with a cryptocrystalline groundmass with leucite microcysts with star-like habit in PPL (**a**) and XPL (**b**). (**c**) Pozzolane Rosse from sample VIR6: porphyritic texture, a big euhedral leucite crystal (bottom right) and small clinopyroxenes (green) at PPL. The cryptocrystalline groundmass shows leucite microcysts with star-like habit. (**d**) Flint used as aggregate in sample VIR7, layer 3 (XPL). (**e**) Ceramic fragment in sample VIR8, PPL. (**f**) Pozzolanelle scoria in sample VIR13, characterised by the abundance of clinopyroxene crystals (at XPL). (**g**) Volcanic rock fragment with holocrystalline groundmass of clinopyroxene and opaques and phenocrysts of leucite in sample VIR15 (PPL). (**h**) A crystal of sanidine, with typical Carlsbad twinning, dispersed in the binder of sample VIR17 close to an altered crystal of clinopyroxene (XPL).

Samples VIR9 and VIR10 present a similar composition; the main difference is the presence of a finishing layer in VIR10 constituted by calcite, with an average thickness of 600 µm. Concerning VIR9 and the second layer of VIR10, they both present an amorphous binder and are characterised by the presence of natural materials with pozzolanic behaviour as the aggregate. In both cases, it is possible to recognise the presence of Pozzolane Rosse pyroclastic products as the major component, and the binder-to-aggregate ratio is 1:3.

3.1.2. La Rinascente

The samples collected in the La Rinascente area can be divided into five new groups. Group 7 comprises samples VIR11 and VIR12, which have a calcic lime binder and an

aggregate composed of a mix of ceramic fragments and Pozzolane Rosse. Sample VIR13 constitutes group 8, and it is characterised by an amorphous binder and different types of pozzolan as aggregate. Sample VIR14 is part of group 5 along with sample VIR8 from the Villa Medici area; the only distinction is related to the finishing layer, which is still present in VIR14 and is absent in VIR8. Sample VIR15 has the same characteristics as samples from group 3. Sample VIR16 constitutes another group (9), as it is composed of two layers, one with an amorphous binder and one with a calcic lime binder, both with Pozzolane Rosse and ceramic fragments. Group 10 is constituted by sample VIR17, which has a calcic lime binder and Pozzolane Rosse aggregate as other groups but differs by the presence of sanidine. Group 11 comprehends samples 1Y, 2Y and 3Y and is characterised by a calcic lime binder, big ceramic fragments and generally fine pozzolan.

VIR11 and VIR12 have a calcic lime binder, which underwent reprecipitation of calcite, particularly evident by the presence of big calcite crystals filling porosities (Figure 3e) and an aggregate constituted by both artificial and natural materials with pozzolanic behaviour. The coarse fraction of the aggregate is constituted by ceramic fragments, which are almost absent as a fine fraction in VIR12. Pozzolane Rosse pyroclastic products constitute the most abundant component of natural materials with pozzolanic behaviour. The binder-to-aggregate ratio is 1:3.

VIR13, collected close to VIR11 and VIR12, presents instead an amorphous binder. The aggregate is mainly composed of Pozzolane Rosse (one clast, including a leucite-bearing granular rock), but also a Pozzolane Nere scoria and a Pozzolanelle scoria (Figure 4f) have been identified (pyroclastic rock fragment with abundant clinopyroxene and euhedral leucite phenocrysts). The binder-to-aggregate ratio is 1:3.

Sample VIR14 (collected close to an incision reporting "1651") is composed of two layers. The first one (most superficial) is a discontinuous plaster layer, ~200 µm thick, characterised by a calcic lime binder and small aggregate fragments, brown-reddish in colour, not optically resolvable. The second layer has an amorphous binder with areas with recrystallised calcite. The aggregate has a pozzolanic behaviour, and it is both natural (Pozzolane Rosse) and artificial (ceramic fragments). The binder-to-aggregate ratio is 1:2.

Sample VIR15 has a microsparitic calcic lime binder, and areas with secondary precipitation of calcite are also present. The aggregate is mainly constituted by Pozzolane Rosse pyroclastic products and Pozzolane Nere, but also volcanic rock fragments with holocrystalline groundmass of clinopyroxene and opaques and phenocrysts of leucite (Figure 4g). The binder-to-aggregate ratio is 1:3.

Sample VIR16 is composed of two layers: the first one (most superficial) has an amorphous binder, and the second a calcic lime binder (Figure 3h). Concerning the aggregate, both layers contain Pozzolane Rosse and ceramic fragments, but the second layer also contains one big fragment of volcanic rock, characterised by phenocrysts of clinopyroxene, olivine and leucite in a cryptocrystalline groundmass. The binder-to-aggregate ratio is 1:3 in both layers.

Sample VIR17 macroscopically presents a white, very thin, superficial layer that was not possible to preserve in the preparation of the thin section, so the description of the sample concerns only the layer below. The binder is a calcic lime binder, and the aggregate is composed mainly of natural materials with pozzolanic behaviour, in particular, Pozzolane Rosse. Of note is the presence of sanidine crystals dispersed in the binder (Figure 4h). The binder-to-aggregate ratio is 1:3.

The samples collected from Aqueduct Y (1Y, 2Y, 3Y) represent what is classically called *cocciopesto*, as they present a coarse aggregate fraction of centimetric dimension constituted by ceramic fragments (Figure 5). They have a calcic lime binder, constituted by micritic calcite, which is not homogeneous due to different interference colours. Ceramic fragments constitute most of the aggregate, and they are also present as powder. Also, pyroclastic and porphyritic rock fragments, presenting a cryptocrystalline groundmass with leucite microcrysts with star-like habit and irregular porosities frequently filled with calcite, are present. The binder-to-aggregate ratio is 1:3.

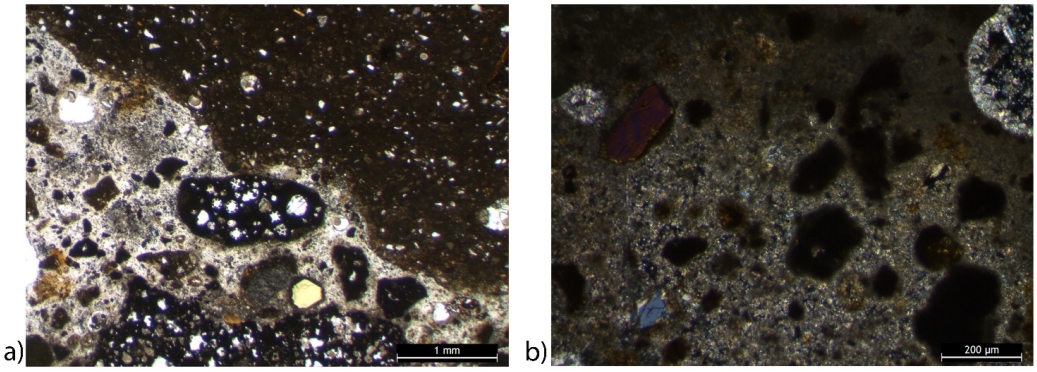

Figure 5. Images at OM of samples from Aqueduct Y. (**a**) Image at PPL of sample 1Y, showing the presence of a big ceramic fragment on top right, but also of pozzolans, with a smaller dimension. (**b**) Image at XPL of sample 2Y, showing the calcic lime binder, and on top right a pore with calcite recrystallisations.

3.2. XRPD

The results of XRPD analyses are shown in Table 2, and diffractograms for each group of samples are presented in Figure S1.

Table 2. Mineral assemblage of mortar samples and relative abundances (++++ very abundant; +++ abundant; ++ common; + present; tr. trace; - not detected). Cal: calcite, Anl: analcime, Lct: leucite, Cpx: clinopyroxenes, Bt: biotite, Qtz: quartz, Gp: gypsum, Vtr: vaterite.

	Sample	Cal	Anl	Lct	Cpx	Bt	Qtz	Gp	Vtr
Group 1	VIR1	-	+++	+	++	-	-	-	-
	VIR2	-	++	++	+++	++	+	-	-
Group 2	VIR3	++	++	-	++	++	-	-	-
Group 3	VIR4	+++	+++	++	++	tr.	+	-	-
	VIR5	+++	+++	tr.	+++	tr.	-	-	-
	VIR6	+++	+	+	+++	tr.	-	-	-
Group 4	VIR7	+++	++	+	++	-	-	-	-
Group 5	VIR8	-	++	-	++	+	+++	-	-
Group 6	VIR9	-	+	+++	+++	tr.	tr.	-	-
	VIR10	++++	++	+	++	tr.	-	-	-
Group 7	VIR11	+++	++	+	++	-	+	+	-
	VIR12	++++	+	+	++	-	-	-	-
Group 8	VIR13	+	+	+++	+++	+	-	-	-
Group 5	VIR14	++	++	+	+++	-	+	-	-
Group 3	VIR15	+	+	++	+++	-	-	-	tr.
Group 9	VIR16	-	++	tr.	++++	+	-	-	-
Group 10	VIR17	+++	++	+	+++	-	+	-	-
Group 11	1Y	+++	+	-	++	-	++	-	-
	2Y	++++	tr.	-	+	tr.	tr.	-	-
	3Y	++++	+	-	++	-	+	-	-

Samples from group 1 show the presence of feldspathoids, such as analcime and leucite, which is in agreement with the presence of pyroclastic rock fragments of the Roman Comagmatic Province [30], and in particular with Pozzolane pyroclastic flows [31], as analcimisation naturally occurs in leucite crystals, being K substituted by Na [20,32]. The presence of clinopyroxene is common to both samples of this group, whereas only VIR2 shows the presence of biotite and quartz.

Sample VIR3 differs from the previous group because of the presence of calcite due to superficial secondary precipitation (see Table S1) and the absence of leucite and quartz.

Group 3 is characterised by abundant calcite, variable abundances of feldspathoids, clinopyroxene from present to abundant and traces of biotite. In sample VIR15, traces of vaterite, a polymorph of $CaCO_3$, were also detected.

Sample VIR7 shows the contribution of all three different strata, and the phases detected are also, in this case, calcite, analcime, leucite and clinopyroxene.

Group 5 shows variable abundances of quartz in its samples, and this might be related to the ceramic fragment composition and abundance in the sampled part that underwent the analysis. The presence of calcite in VIR14 must be linked to the presence of a calcic superficial layer. Analcime and clinopyroxene are common in both samples, but leucite is present only in VIR14 and biotite only in VIR8.

Samples from group 6 are similar (feldspathoids, clinopyroxene and traces of biotite) except for the abundant presence of calcite in VIR10, which must be due to the presence of a calcic superficial layer, as the layer below has an amorphous binder, and the traces of quartz detected in VIR9.

Group 7 is characterised by abundant to very abundant calcite, scarce to present analcime, scarce leucite and present clinopyroxene. Moreover, sample VIR11 also contains quartz and gypsum: quartz can be due to the presence of flint in the aggregate, as detected at OM (see Table S2), and gypsum can be interpreted as an alteration product due to the sulphation of the calcic binder [33].

In sample VIR13 (group 8), the presence of calcite is due to superficial secondary precipitation (see Table S1), and the other mineralogical phases detected do not differ from the ones previously described (feldspathoids, clinopyroxene and biotite).

Sample VIR16 (group 9) is composed of analcime, traces of leucite, very abundant clinopyroxene and present biotite. The absence of calcite should be related to the point of sampling for obtaining the XRPD powder: macroscopically, the sample does not show a clear stratigraphy, and probably only the layer with an amorphous binder was sampled.

Sample VIR17 (group 10) shows abundant calcite and clinopyroxene, present analcime and scarce leucite and quartz.

Group 11 is characterised by a content of calcite that goes from abundant to very abundant, and the clinopyroxene has been detected as present or scarce. The most interesting aspect is the lower abundance of feldspathoids, as well as the presence in all three samples of quartz. This is in agreement with the paucity of pyroclastic rock fragments found in these samples and the abundance of ceramic fragments.

3.3. SEM-EDS

The SEM-EDS analyses reported in this section focus on the main feature useful for a deeper understanding of the materials used as aggregate, the composition of the binder and the reaction that occurred between aggregate and binder. More details about the characterisation are given in Figure S2.

The pozzolanic material (i.e., Pozzolane Rosse, Pozzolane Nere and Pozzolanelle) is characterised by the presence of leucite. The results at XRPD, however, also show the presence of analcime, a mineral phase that can be related to the analcimisation of leucite. SEM-EDS confirmed the presence of both leucite and analcime in the pozzolanic aggregate fragments, as in some cases, EDS analyses show the presence (in order of intensity of the peaks) of Si, Al and K (indicating the composition of leucite), whereas in other cases, K is substituted by Na (indicating analcime presence) (Figure 6). In each sample investigated, these two mineral phases were present. Some pozzolanic fragments showed the presence of only analcime, some others of only leucite, and others both at the same time; in a few cases, it was also possible to observe the transformation of a leucite crystal into analcime, as it presents a core rich in K and external borders in which the intensity of K peak decreases and Na appears. In sample VIR6, in a pozzolanic fragment presenting leucite and analcime at the same time, melilite has also been detected (Figure 6, image 5), which is a characteristic phase of Colli Albani products [34,35]. The habit of the crystals has been checked to see if it is related to the presence of one of the two phases, but no correlation has been found:

in fact, euhedral crystals can be constituted by leucite or analcime as well as crystals with star-like habit.

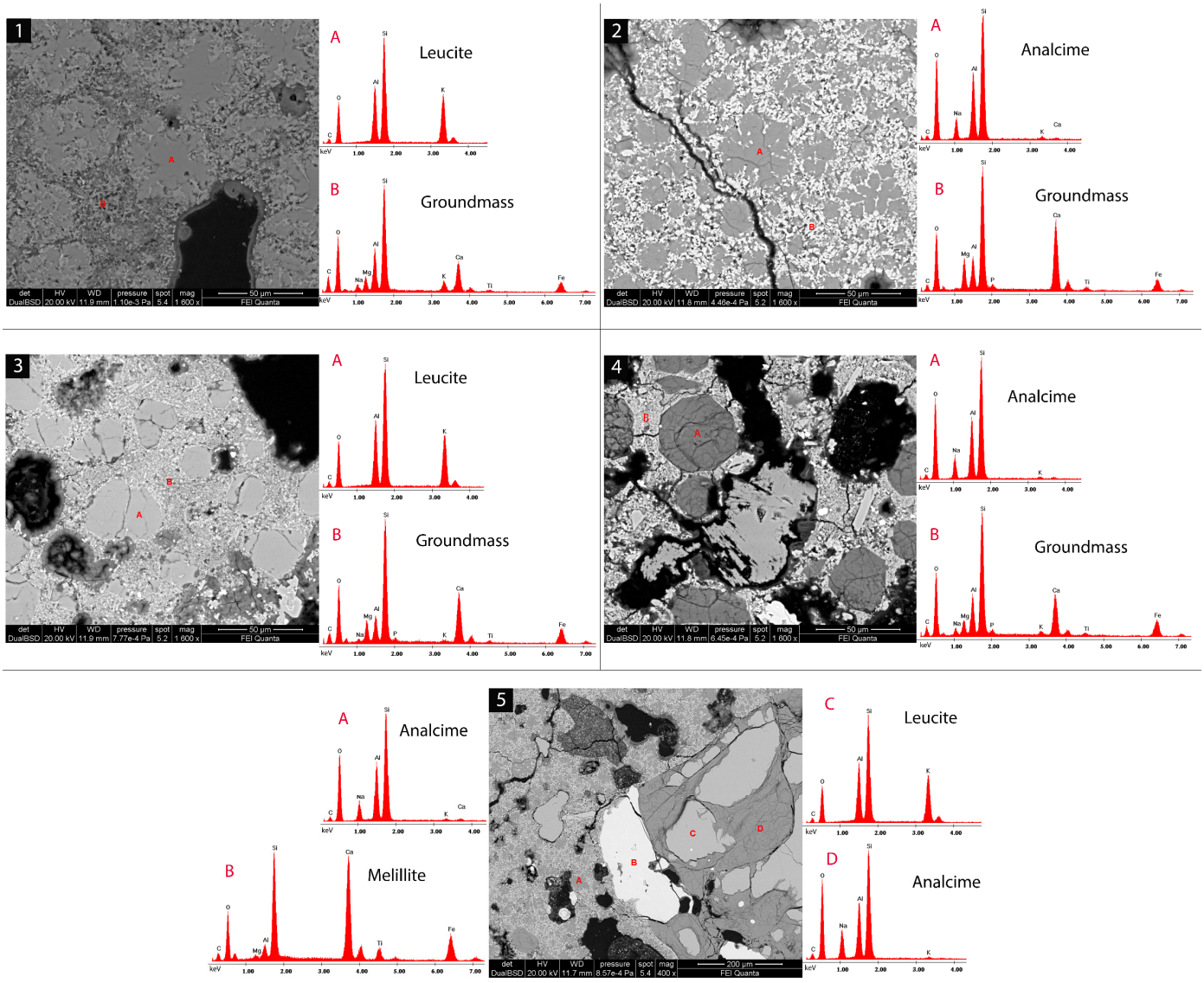

Figure 6. SEM-EDS analysis on the pozzolanic aggregate. The groundmass is always characterised by an intense peak of Si, followed by Ca and Al, and then smaller peaks of Mg and Fe, always a very small peak of Ti, and occasionally also K, Na and P. Image **1** (VIR1) shows leucite with star-like habit and the relative spectra, whereas in image **2** (VIR10, second layer), analcime with the same star-like habit is visible. Image **3** (VIR7, second layer) still shows the presence of leucite, with euhedral habit, and in image **4** (VIR7, second layer), a crystal with the same shape is present, but the spectra reveal it is analcime. Image **5** (VIR6) shows a pyroclastic rock fragment presenting mainly analcime with star-like habit; phenocrysts are constituted by melilite and a crystal of leucite transforming into analcime.

SEM-EDS observations on the pozzolanic aggregate also allowed us to identify the presence of recrystallisations inside the aggregate pores. These recrystallisations appear as acicular crystals or uniform filling of the pore. Sometimes, two layers are present independently in the form of recrystallisation. The EDS spectra show that the acicular crystals are mainly composed of Si and Al, and small peaks of Ca and K are present (VIR1, VIR10, VIR13, VIR16), whereas the border that is interposed between the crystals and the groundmass when present, shows the presence of Mg (VIR1) (Figure 7a); there are few exceptions in which Mg is also present in the acicular crystals, and one exception in which

K is missing (VIR15). When the pores are uniformly filled with recrystallisations, generally only the Ca peak is present (VIR6, VIR7); an exception has been detected in sample VIR15 in which the filling has the same composition of acicular crystals (Si, Al, Ca, K) (Figure 7b). The border between the Ca filling in the pore and the groundmass has been investigated in sample VIR6, which shows the highest peak for Si and Al and smaller peaks for many elements, such as Ca, K, Fe and Mg.

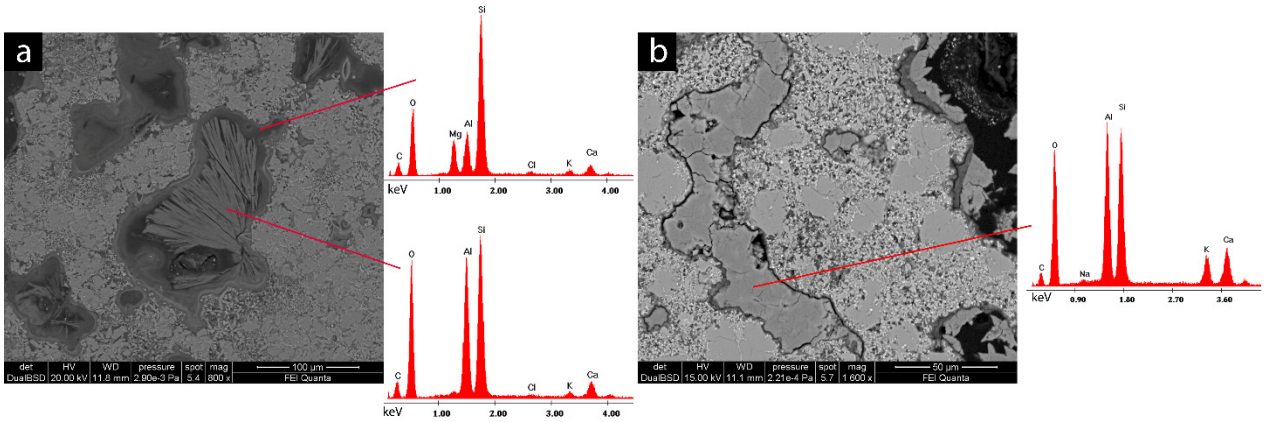

Figure 7. Recrystallisation in the pores of the aggregate observed at SEM-EDS. (**a**) Acicular crystals in sample VIR1, with also a border interposed between them and the groundmass. (**b**) Uniform filling of a porosity in VIR15.

The binder morphology and chemical composition have been investigated through SEM-EDS analyses. As attested by OM and XRPD, some samples present a calcic lime binder, whereas others have an amorphous one. Moreover, there are some finishing layers (VIR7 layer 1, VIR10 layer 1) that at OM show crystals of calcite, for which the presence of Ca has been confirmed by SEM-EDS and which look more compact with respect to the layers below them. VIR14 layer 1 is also a finishing layer, but with respect to the ones previously described, it also contains a small fraction of aggregate, which, thanks to SEM-EDS, was possible to identify as pozzolan fragments and single crystals dispersed in the calcic binder (Figure 8, image 1). Concerning the samples investigated at SEM-EDS, in the ones with a calcic lime binder, the presence of Ca is confirmed, and the morphology is microcrystalline. However, there are areas in which the intensity of the Ca peak decreases, and peaks of Si and Al appear; they generally look less bright than the areas rich in Ca. For the layers showing an amorphous binder, the chemical composition is generally characterised by Si as a major peak, followed by Al, and then the variable intensity of Ca and Mg, a small peak of K, and sometimes also Na and Fe. Sample VIR13 presents some highly altered areas in the binder, in which the presence of S has been detected, and also some areas with elongated crystals of calcite (hundred µm dimension), which EDS confirmed to be composed of Ca. Moreover, some needle-shaped crystals have been identified in the binder of sample VIR1, which is a layer with an amorphous binder. This needle conformation has also been detected at the borders of an altered area in the amorphous binder of sample VIR16 layer 2. The spectra of these needle-shaped crystals show the presence of Si, Al, Ca, K and Mg (Figure 8, image 3). Some other needle-shaped crystals have been identified in sample VIR15; in this case, the border of the crystals is more jagged, and the spectra show the presence of Al, Ca and Si.

The contact areas between the different layers of the same samples have been investigated. In sample VIR7, the area of layer 2 directly in contact with layer 1 is more enriched in Ca, especially in some areas that protrude from the most external border and penetrate deeper into the layer (Figure 8, image 4). In sample VIR16, the area of contact between the two layers is composed of Si, followed by Al and Mg, and smaller peaks of Ca and K are also present. In samples VIR10 and VIR14, the layers are clearly separated.

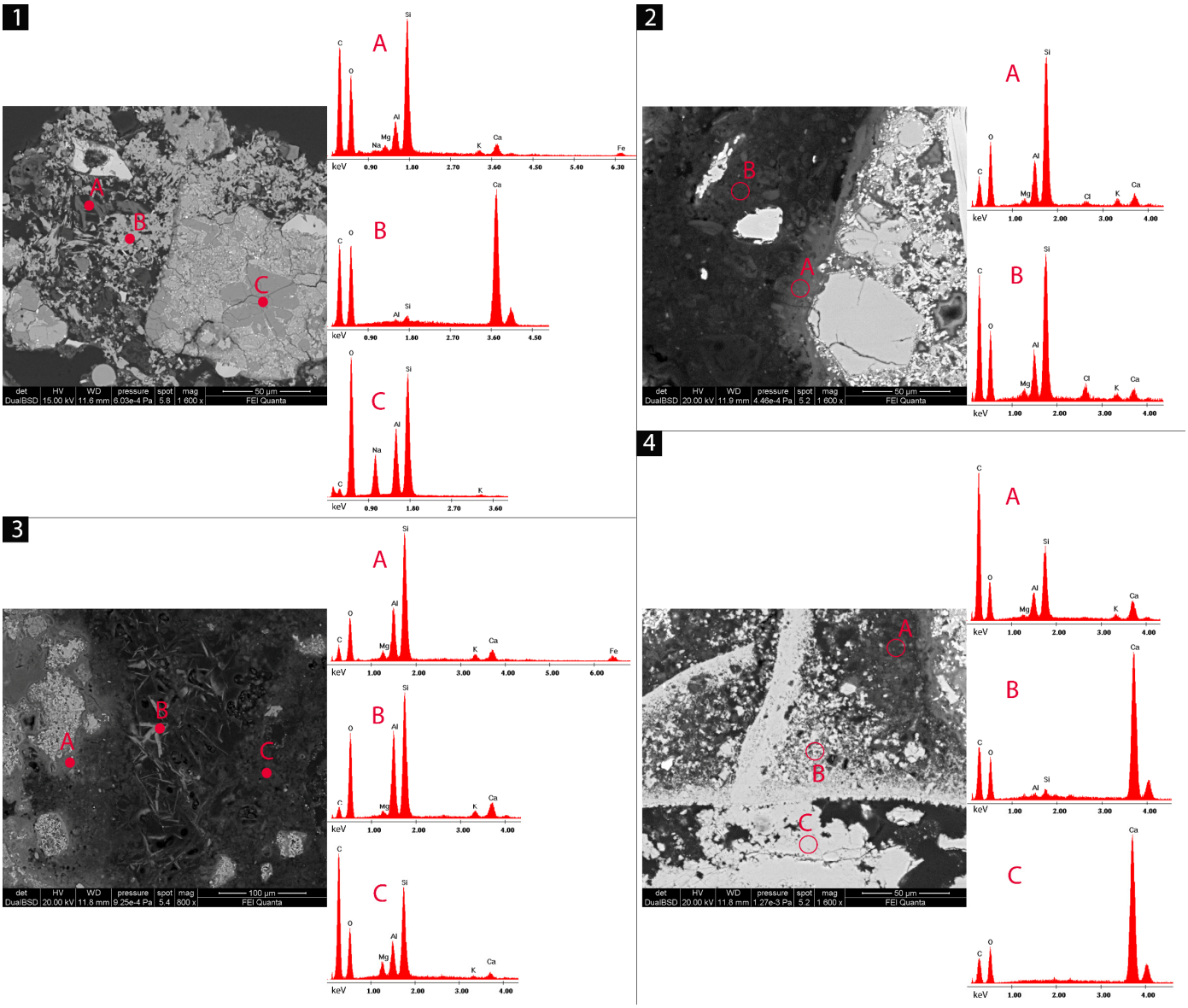

Figure 8. SEM-EDS analysis on the binder. Image (**1**) shows the first layer of VIR14, which has a calcic binder (**B**) but also presents some needle-shaped crystals (**A**) rich in Si and characterised also by the presence of Al, Ca, Mg, Na, K, Fe; the aggregate is constituted by single crystals and pozzolan fragments (in this case containing analcime, point (**C**). Image (**2**) shows the reaction rim (**A**) and the amorphous binder (**B**) in sample VIR10: no significative differences are visible in the spectra, and Cl is due to the resin used to realise the thin sections. In image (**3**), some needle-shaped crystals (**B**) are present between an area enriched in Fe (**A**) and the amorphous binder (**C**) of sample VIR1. In image **4**, the interface between layer 1 (at the bottom of the picture) and layer 2 is shown: substantial difference is shown between spectra (**A**,**B**), even if both belong to a layer with calcic lime binder, whereas layer 1 is uniform and the spectrum (**C**) shows the presence of Ca.

In general, what the SEM-EDS analyses on the binder have highlighted is that even in the samples with a calcic lime binder, which is very common according to the literature, many alterations have occurred, and the presence of calcite is not homogeneous. There are, in fact, areas characterised by a prevalence of Si and Al with respect to Ca, which is also an aspect that characterises the amorphous binders that are less common and studied. Because of the inhomogeneity of the calcic lime binder, it is also less probable to find defined reaction rims between the aggregate with pozzolanic behaviour (both natural and

artificial) and the binder, which is something commonly reported in the literature regarding air hardening binders with the addition of materials providing hydraulic characteristics. Even when these rims were found, no significant variations regarding the proportion of the peaks of the elements were found (Figure 8, image 2).

4. Discussion

The archaeometric characterisation of mortar samples from *Aqua Virgo* and Aqueduct Y allowed us to investigate the materials used for masonries that are supposed to remain in contact with water and determine differences and analogies in the materials of different interventions.

The chronology of the different phases of interventions is complex due to the fact that *Aqua Virgo* has operated since 19 BC, and Aqueduct Y's origin is still unknown. Despite this, the archaeometric characterisation of the mortars allowed us to obtain some grouping between the samples.

The data collected at OM and XRPD allowed us to clearly differentiate the samples from Aqueduct Y from those of *Aqua Virgo* and, in particular, from samples from group 5 because of a different type of binder (calcic lime binder for group 11 and amorphous for group 3), and from samples from group 7 because in this latter group there is a higher variability in the aggregate (not only pozzolans and ceramic fragments). This is in agreement with the archaeological data: Aqueduct Y does not show a stratigraphy of interventions on the walls of the inner duct, suggesting that the samples belong to the original construction phase, whereas samples from group 5 were both collected close to incision attesting that they were realised in the 17th century, and samples from group 7 were collected in an area that underwent interventions.

Concerning *Aqua Virgo*, the samples that archaeologically can be attributed to the Roman phase of construction are the ones of group 3, with samples VIR4-6 being collected from a well and a vault architectonically compatible with the techniques of construction of ancient Romans and VIR15 being collected from the core of the wall, close to a lead pipe. All these samples are characterised by the presence of a calcic lime binder, an aggregate mainly composed of natural materials with pozzolanic behaviour, and, in particular, Pozzolane Rosse and Pozzolane Nere, and a binder-to-aggregate ratio of 1:3. However, the analyses highlighted some differences: sedimentary carbonate rocks are present in samples VIR4-6 and absent in sample VIR15; VIR15 contains a fragment of mortar and the other samples do not; VIR4-6 have lumps, which are absent in VIR15. These dissimilarities can be due to the different functions of these mortars and the fact that they come from distant areas (Villa Medici and La Rinascente) of the *Aqua Virgo*, which might have had an influence on the materials available.

Another aspect to consider is the type of material used to induce hydraulicity in the mortar. The majority of the samples investigated contain main aggregate natural materials with pozzolanic behaviour, independently from the group. In fact, in the samples in which artificial materials with pozzolanic behaviour have been identified, pozzolans are present. The widespread presence of pozzolans is due to several factors. Their use in hydraulic mortars has been attested since Roman times; several authors, such as Vitruvius, Pliny the Elder and Strabo, testify about their employment and praise their use for hydraulic mortars [25]. This type of material is widely available in the city of Rome, as the geological setting of the Roman Comagmatic Region is characterised by its presence [36,37]. This, unfortunately, constitutes a problem in identifying the different construction phases: even the samples that report an incision with a date referring to a later intervention contain pozzolans, as well as the ones related to the Roman construction phase. The preferential use of Pozzolane Rosse that the literature reports to be practised by Romans between the end of the 2nd century BC and the beginning of the 1st century AD [38] cannot be used as the only criteria to determine the dating of the samples, as also samples explicitly belonging to later interventions (VIR7, VIR14) present Pozzolane Rosse as main aggregate.

However, by applying a multi-analytical approach and cross-checking the data obtained, it was possible to make groups. Samples VIR1 and VIR2 have an analogous composition (group 1), whereas VIR3, which was collected close to the other two, presents a slightly different aggregate composition, which suggests that it belongs to a different phase of intervention (group 2). Samples VIR4-6 from Villa Medici area belong to group 3, as well as sample VIR15 from La Rinascente area, and these are the samples that, according to the archaeological evidence, are most probably related to the original Roman phase of construction, as stated above. Sample VIR7 (group 4) is the only one in which three layers have been identified, and the most peculiar one is the third, in which a big fragment of flint has been identified; as it reports the incised date, it can be used as a reference for the interventions of 1742. Also, VIR8 (Villa Medici area) and VIR14 (La Rinascente area) have an incision, reporting, in the first case, "1650" and, in the second, "1651"; they both belong to group 5 as they present an amorphous binder, have natural and artificial pozzolanic aggregate and the binder-to-aggregate ratio is 1:2. Group 6 is composed of sample VIR9 and VIR10, being the main features an amorphous binder and Pozzolane Rosse as aggregate, which indicates a slight difference with group 1 in which also Pozzolane Nere are present. Samples VIR11-13 were collected in the same area, but only VIR11 and VIR12 (group 7), which are bedding mortars that have the same characteristics (calcic lime binder, ceramic fragments among the aggregate, marble fragments); VIR13, which is the covering layer on top of VIR12, differs from the other two because of its amorphous binder and the absence of ceramic fragments. Concerning sample VIR11, gypsum has been detected through XRPD: the presence of this mineral phase can be due to the degradation action of sulfuric acid, which is commonly present in atmospheric water and induces a sulphation process in the lime-based mortar, which produces gypsum [20]. Sample VIR16, which macroscopically looks similar to sample VIR14 (and they both come from La Rinascente area), after the archaeometric investigation must be considered as belonging to a different group: they both have two layers, but the mineralogical composition and the binder are different. Finally, sample VIR17, which comes from the same vault as sample VIR5-6, is similar in composition to these two samples but differs because of the presence of sanidine in the aggregate and the absence of sedimentary carbonate rock. All the data collected through this characterisation allowed us to create some grouping and differentiate among interventions that just observed macroscopically looked similar.

The combination of OM, XRPD and SEM-eds analyses allowed us to investigate an interesting aspect of the mortars under study: the amorphous binder in some of the samples from *Aqua Virgo*. The presence of an amorphous binder is not related to the type of aggregate, as it has been found both in samples with natural and artificial materials with pozzolanic behaviour. The only aspect that all the samples with this type of binder have in common is the closeness to water. All the samples collected from the vault (VIR4-6, VIR17), from high points in the lateral walls (VIR7, VIR16), or from the inner part of the walls (VIR11-12, VIR15), which are the areas less exposed to the contact with water, present a calcic lime binder. The samples with an amorphous binder, as demonstrated by OM, are the ones collected from the lateral walls in points still very close to water (VIR1-3, VIR8-10) or that were close to water in the past (VIR13-14, VIR16). XRPD analyses do not always confirm the absence of calcite, but as explained in the results, the reason is related to the presence of precipitation of secondary calcite (VIR3, VIR13) or because of the presence of finishing layers containing calcite (VIR10, VIR14). SEM-EDS analysis revealed that the amorphous binder is generally characterised by Si as a major peak, followed by Al, and then Ca and Mg, a small peak of K, and occasionally Na and Fe. The absence of calcite in the binder constitutes a rare case, as usually, even if the mortar is hydraulic, precipitation of calcite occurs [20]. There are some exceptions reported in the literature [12,39], in which the presence of an amorphous binder and the absence of calcite are justified by the hydraulic reaction that occurred between the aggregate with pozzolanic behaviour (mainly natural) and the lime that resulted in the formation of C-A-S-H binding phase with wispy halos and tendril-like strands, which remained reactive long after hydrated lime was consumed.

In particular, the dissolution of leucite crystals has been considered a source of Al and K, which are then incorporated into the binder, causing a substantial reconfiguration of the C-A-S-H [39]. Considering that between all the parameters that can influence the hydraulic reaction in lime-based mortars (availability of reactive silica and alumina, reactive surface of the aggregate) [40], the only one that mainly variates is the exposure to water, in this case study, it must be considered an important factor in the formation of the amorphous binder. In sample VIR1, it was also possible to see needle-shaped crystals in the binder, whose composition is analogous to the one described above for the amorphous binder; these needle-shaped crystals, with the same composition, have also been found in small areas of sample VIR16 layer 2, which has a calcic lime binder. The presence of these particular structures can be linked to the formation of hydraulic phases in the binder due to the use of alumina-rich Pozzolane Rosse: analogous microstructures, sometimes also identified as blade-like cementitious gels, have been described in ancient Roman pozzolanic mortars [31,41]. The chemical and microstructural characteristics of Pozzolane Rosse may induce a high reactivity with the lime, forming very low Ca/Si calcium–aluminate–silicate hydrate (CASH) [42].

The detection of traces of vaterite through XRPD in sample VIR15 is another unusual result. Vaterite is a polymorph of $CaCO_3$, which is metastable at ambient conditions; however, the presence of metal ions or organic matter can stabilise it. The XRPD spectra of the sample show that calcite is scarcely present, and there are no other phases except these two that can be related to the binder. The microstructure of the binder, observed at SEM-EDS, shows a particular morphology with a needle-shaped structure, and chemical analyses revealed the presence of Al, Ca and Si (in order of intensity), which was not observed in other samples. The presence of vaterite can be due to a process of self-healing of the lime mortars in a wet and dry cycle [43], as the one that might have occurred considering that the sample has been collected inside the duct of the aqueduct, close to a pipe, in the inner part of the wall, and the stabilisation of vaterite can be due to the presence of Al [44].

5. Conclusions

The archaeometric characterisation of the mortars coming from the inner duct of *Aqua Virgo* and Aqueduct Y is the first scientific study regarding the building materials used in the only Roman aqueduct, among the eleven built for the city of Rome, that never stopped working since 19 BC and the unknown aqueduct located below it in the La Rinascente area.

Due to its longevity, *Aqua Virgo* is now the result of several building phases that lay one on top of the other, making the interpretation of the different interventions very complex. This work constitutes the first step toward the classification of different mortar groups in order to establish a relative chronology. Integrating the archaeological evidence and incisions left by labourers on the walls with the archaeometric characterization of the mortars, it was possible to obtain some grouping that can constitute a base with whom to compare other samples from the same aqueduct in order to reconstruct its history. All the samples from Aqueduct Y can be classified as *cocciopesto* and are representative of the original phase of construction. Concerning *Aqua Virgo*, Pozzolane Rosse was a type of aggregate used in every phase of construction, from antiquity to more recent times (18th century): their use was widespread already in Roman times for the realisation of high-quality hydraulic mortars, and their availability in the area made it a timeless material in this type of constructions, always in contact with water.

The presence, in some samples, of a calcic lime binder and in others of an amorphous one gave the opportunity to evaluate the differences between them in order to detect the factor responsible for this differentiation. All samples contain an aggregate inducing hydraulicity to the mortar, and the presence of natural or artificial materials with pozzolanic behaviour was not a discriminant factor for the presence or absence of the amorphous binder, as well as the binder-to-aggregate ratio: further investigations are suggested to disclose the role played by the direct and prolonged contact with water.

This study opens the road for further investigation on mortars from *Aqua Virgo* in order to compare the materials, reconstruct the history of interventions and understand how the prolonged interaction with water affects lime-based mortars with pozzolanic aggregate.

Supplementary Materials: The following supporting information can be downloaded at: https://www.mdpi.com/article/10.3390/buildings14010069/s1, Table S1: Report of the sampling and description of the sample; Table S2: OM characterisation; Figure S1: XRPD results for each group of samples; Figure S2: SEM-EDS analysis on aggregates.

Author Contributions: L.C.: conceptualisation, data curation, formal analysis, investigation, writing—original draft. M.E.A.: formal analysis, investigation, writing—original draft. L.M.: funding acquisition, supervision, writing—review and editing. S.M.: funding acquisition, supervision, writing—review and editing. All authors have read and agreed to the published version of the manuscript.

Funding: This research received no external funding.

Data Availability Statement: All data derived from this research are presented in the enclosed figures and tables.

Acknowledgments: The authors want to express their gratitude to Soprintendenza Speciale Archeologia, Belle Arti e Paesaggio di Roma, in particular to Marta Baumgartner and Sovrintendenza Capitolina ai Beni Culturali. We also want to thank ACEA Ato2 for the support in accessing the still functioning part of *Aqua Virgo*, in particular, Francesco Prisco, and the speleological groups "Sotterranei di Roma" and "Gruppo Speleo Archeologico Vespertilio", which have supported the speleological investigations and collaborated on the creation of detailed maps of the aqueduct.

Conflicts of Interest: The authors declare no conflicts of interest.

References

1. Aicher, P.J. Terminal Display Fountains ("Mostre") and the Aqueducts of Ancient Rome. *Phoenix* **1993**, *47*, 339–352. [CrossRef]
2. Frontinus. *Frontinus: De Aquaeductu Urbis Romae*; Cambridge University Press: Cambridge, UK, 2004; ISBN 978-1-139-45207-6.
3. Ashby, T. *Gli Acquedotti Dell'antica Roma*; Quasar: Roma, Italy, 1991.
4. Quilici, L. *Sull'acquedotto Vergine Dal Monte Pincio Alle Sorgenti*; Quaderni dell'Istituto di Topografia Antica dell'Università di Roma, V: Roma, Italy, 1968.
5. Aicher, P.J. *Guide to the Aqueducts of Ancient Rome*; Bolchazy-Carducci Publishers: Wauconda, IL, USA, 1995.
6. Rinne, K.W. *The Waters of Rome: Aqueducts, Fountains, and the Birth of the Baroque City*; Yale University Press: New Haven, CT, USA, 2011.
7. Annoscia, G. *Fonti e Strutture per La Conoscenza Del Sistema Idrico Di Roma Nel Medioevo*; Aracne Editrice: Roma, Italy, 2008.
8. Nicolazzo, V. *Acqua Vergine a Roma: Acquedotti e Fontane*; Colosseo Grafica Editoriale: Roma, Italy, 1999.
9. Pracchia, S.; Pultrone, M.; Saviane, N. Acquedotti. In *Roma Rinascente. La Città Antica tra Quirinale e Pincio*; De Luca Editori D'arte: Roma, Italy, 2017; pp. 69–91, ISBN 978-88-6557-320-4.
10. Baumgartner, M. *Archeo—Attualità del Passato*; Timeline Publishing: Roma, Italy, 2018; pp. 54–60.
11. Pace, P. *Acquedotti Di Roma e Il De Aquaeductu Di Frontino*, 3rd ed.; Consiglio Nazionale Delle Ricerche: Roma, Italy, 2010.
12. Botticelli, M.; Calzolari, L.; De Vito, C.; Mignardi, S.; Medeghini, L. Aqua Traiana, a Roman Infrastructure Embedded in the Present: The Mineralogical Perspective. *Minerals* **2021**, *11*, 703–719. [CrossRef]
13. Benjelloun, Y.; de Sigoyer, J.; Carlut, J.; Hubert-Ferrari, A.; Dessales, H.; Pamir, H.; Karabacak, V. Characterization of Building Materials from the Aqueduct of Antioch-on-the-Orontes (Turkey). *Comptes Rendus Geosci.* **2015**, *347*, 170–180. [CrossRef]
14. Maravelaki-Kalaitzaki, P.; Galanos, A.; Doganis, I.; Kallithrakas-Kontos, N. Physico-Chemical Characterization of Mortars as a Tool in Studying Specific Hydraulic Components: Application to the Study of Ancient Naxos Aqueduct. *Appl. Phys. A* **2011**, *104*, 335–348. [CrossRef]
15. Rizzo, G.; Ercoli, L.; Megna, B.; Parlapiano, M. Characterization of Mortars from Ancient and Traditional Water Supply Systems in Sicily. *J. Therm. Anal. Calorim.* **2008**, *92*, 323–330. [CrossRef]
16. Figueiredo, M.O.; Veiga, J.P.; Silva, T.P. Materials and reconstruction techniques at the Aqueduct of Carthage since the Roman period. *Hist. Constr. Guimaraes* **2001**, *1*, 391–400.
17. Sabbioni, C.; Zappia, G.; Riontino, C.; Blanco-Varela, M.T.; Aguilera, J.; Puertas, F.; Balen, K.V.; Toumbakari, E.E. Atmospheric Deterioration of Ancient and Modern Hydraulic Mortars. *Atmos. Environ.* **2001**, *35*, 539–548. [CrossRef]
18. Seymour, L.M.; Keenan-Jones, D.; Zanzi, G.L.; Weaver, J.C.; Masic, A. Reactive Ceramic Aggregates in Mortars from Ancient Water Infrastructure Serving Rome and Pompeii. *Cell Rep. Phys. Sci.* **2022**, *3*, 101024. [CrossRef]
19. Pollio, V. *De Architectura*; Edizioni Studio Tesi: Roma, Italy, 2008; ISBN 978-88-7692-382-1.
20. Torraca, G. *Lectures on Materials Science for Architectural Conservation*; Getty Conservation Institute: Los Angeles, CA, USA, 2009; ISBN 978-0-9827668-2-8.

21. Moropoulou, A.; Bakolas, A.; Anagnostopoulou, S. Composite Materials in Ancient Structures. *Cem. Concr. Compos.* **2005**, *27*, 295–300. [CrossRef]
22. Pecchioni, E.; Fratini, F.; Cantisani, E. *Le Malte Antiche e Moderne Tra Tradizione Ed Innovazione*; Pàtron Editore: Bologna, Italy, 2008.
23. Szabó, S.; Funari, M.F.; Lourenço, P.B. Masonry Patterns' Influence on the Damage Assessment of URM Walls: Current and Future Trends. *Dev. Built Environ.* **2023**, *13*, 100119. [CrossRef]
24. Cairoli Giuliani, F. *L'edilizia Nell'antichità*; Carrocci Editore: Roma, Italy, 2018.
25. Lancaster, L.C. *Concrete Vaulted Construction in Imperial Rome: Innovations in Context*; Cambridge University Press: Cambridge, UK, 2005; ISBN 978-0-521-84202-0.
26. Montalbano, R. Inquadramento Topografico. In *Roma Rinascente. La città antica tra Quirinale e Pincio*; De Luca Editori D'arte: Roma, Italy, 2017; pp. 25–38, ISBN 978-88-6557-320-4.
27. Beni Culturali—Normal. *UNI 11176:2006 Cultural Heritage—Petrographic Description of a Mortar*; UNI (Italian National Standards): Milan Italy, 2006.
28. Pecchioni, E.; Fratini, F.; Cantisani, E. *Atlante Delle Malte Antiche in Sezione Sottile al Microscopio Ottico*; Nardini Editore: Firenze, Italy, 2014.
29. Martin, J.D. Using XPowder: A Software Package for Powder X-ray Diffraction Analysis, D.L.GR 1001; Spain. 2004. Available online: https://www.ugr.es/~jdmartin/download/xpowder.pdf (accessed on 22 December 2023).
30. Boari, E.; Avanzinelli, R.; Melluso, L.; Giordano, G.; Mattei, M.; De Benedetti, A.A.; Morra, V.; Conticelli, S. Isotope Geochemistry (Sr–Nd–Pb) and Petrogenesis of Leucite-Bearing Volcanic Rocks from "Colli Albani" Volcano, Roman Magmatic Province, Central Italy: Inferences on Volcano Evolution and Magma Genesis. *Bull. Volcanol.* **2009**, *71*, 977–1005. [CrossRef]
31. Jackson, M.; Deocampo, D.; Marra, F.; Scheetz, B. Mid-Pleistocene Pozzolanic Volcanic Ash in Ancient Roman Concretes. *Geoarchaeology Int. J.* **2010**, *25*, 36–74. [CrossRef]
32. Giampaolo, C.; Lombardi, G. Thermal Behaviour of Analcimes from Two Different Genetic Environments. *Eur. J. Mineral.* **1994**, 285–290. [CrossRef]
33. Ciriaco, G.; Godano, R.F.; Di Sabatino, B.; Barrese, E. The Alteration of Leucite-Bearing Rocks: A Possible Mechanism. *Eur. J. Mineral.* **1997**, 1277–1292. [CrossRef]
34. Gaeta, M.; Freda, C.; Marra, F.; Arienzo, I.; Gozzi, F.; Jicha, B.; Di Rocco, T. Paleozoic Metasomatism at the Origin of Mediterranean Ultrapotassic Magmas: Constraints from Time-Dependent Geochemistry of Colli Albani Volcanic Products (Central Italy). *Lithos* **2016**, *244*, 151–164. [CrossRef]
35. Conticelli, S.; Boari, E.; Benedetti, A.A.; Giordano, G.; Mattei, M.; Melluso, L.; Morra, V. Geochemistry, Isotopes and Mineral Chemistry of the Colli Albani Volcanic Rocks: Constraints on Magma Genesis and Evolution. In *The Colli Albani Volcano*; Geological Society of London: London, UK, 2010; pp. 107–139.
36. Luberti, G.M.; Marra, F.; Florindo, F. A Review of the Stratigraphy of Rome (Italy) According to Geochronologically and Paleomagnetically Constrained Aggradational Successions, Glacio-Eustatic Forcing and Volcano-Tectonic Processes. *Quat. Int.* **2017**, *438*, 40–67. [CrossRef]
37. Marra, F.; Danti, A.; Gaeta, M. The Volcanic Aggregate of Ancient Roman Mortars from the Capitoline Hill: Petrographic Criteria for Identification of Rome's "Pozzolans" and Historical Implications. *J. Volcanol. Geotherm. Res.* **2015**, *308*, 113–126. [CrossRef]
38. Marra, F.; D'Ambrosio, E.; Gaeta, M.; Mattei, M. Petrochemical Identification and Insights on Chronological Employment of the Volcanic Aggregates Used in Ancient Roman Mortars. *Archaeometry* **2016**, *58*, 177–200. [CrossRef]
39. Seymour, L.M.; Tamura, N.; Jackson, M.D.; Masic, A. Reactive Binder and Aggregate Interfacial Zones in the Mortar of Tomb of Caecilia Metella Concrete, 1C BCE, Rome. *J. Am. Ceram. Soc.* **2022**, *105*, 1503–1518. [CrossRef]
40. Dilaria, S.; Secco, M.; Bonetto, J.; Ricci, G.; Artioli, G. Making Ancient Mortars Hydraulic. How to Parametrize Type and Crystallinity of Reaction Products in Different Recipes. In Proceedings of the Historic Mortars International Conference, Ljubljana, Slovenia, 21–23 September 2022; Springer: Berlin/Heidelberg, Germany; pp. 36–52.
41. Jackson, M.D.; Logan, J.M.; Scheetz, B.E.; Deocampo, D.M.; Cawood, C.G.; Marra, F.; Vitti, M.; Ungaro, L. Assessment of Material Characteristics of Ancient Concretes, Grande Aula, Markets of Trajan, Rome. *J. Archaeol. Sci.* **2009**, *36*, 2481–2492. [CrossRef]
42. Hong, S.-Y.; Glasser, F.P. Alkali Sorption by C-S-H and C-A-S-H Gels Part II. Role of Alumina. *Cem. Concr. Res.* **2002**, *32*, 1101–1111. [CrossRef]
43. Singh, M.; Vinodh Kumar, S.; Waghmare, S.A.; Sabale, P.D. Aragonite–Vaterite–Calcite: Polymorphs of $CaCO_3$ in 7th Century CE Lime Plasters of Alampur Group of Temples, India. *Constr. Build. Mater.* **2016**, *112*, 386–397. [CrossRef]
44. Li, J.; Yu, Q.; Huang, H.; Yin, S. Effects of Ca/Si Ratio, Aluminum and Magnesium on the Carbonation Behavior of Calcium Silicate Hydrate. *Materials* **2019**, *12*, 1268. [CrossRef]